J Mater Sci: Mater Med (2011) 22:1663–1670
DOI 10.1007/s10856-011-4338-z

Preparation and characterization of biomimetically and electrochemically deposited hydroxyapatite coatings on micro-arc oxidized Ti–13Nb–13Zr

Laís T. Duarte · Sonia R. Biaggio · Romeu C. Rocha-Filho · Nerilso Bocchi

Received: 29 January 2011 / Accepted: 29 April 2011 / Published online: 12 May 2011

Abstract Surface properties and corrosion resistance analyses of Ti–13Nb–13Zr coated by an oxide film (obtained by micro-arc oxidation at 300 V) or an oxide/hydroxyapatite (HA) film are reported. HA films were biomimetically or electrochemically deposited on the alloy/oxide surface, and their properties compared. Both the biomimetic and the electrochemical method yielded rough and globular apatite surfaces (10–20 μm globules for the former and 1–2 μm for the latter). As inferred from XRD data, the electrochemical method yielded more biologic-like HA films, while the biomimetic method yielded films containing a mixture of calcium phosphate phases. Coated Ti–13Nb–13Zr samples were immersed in an aerated PBS solution and continuously analyzed during 49 days. Considering that, after immersion, the biomimetically deposited films presented smaller variations in thickness and morphology and higher electric resistance (determined by electrochemical impedance spectroscopy), they clearly provide significantly better protection to the Ti–13Nb–13Zr alloy when in PBS solution.

1 Introduction

Titanium and some of its alloys are promising materials for implants because of the following characteristics, among others: high corrosion resistance, non-toxicity, and mechanical properties compatible to bones [1]. Titanium, niobium, and zirconium, which belong to a group of elements known as *valve metals*, usually have their surfaces covered by a thin oxide film spontaneously formed in air or in electrolyte solutions at open circuit; this film constitutes a barrier between the metal and the medium. When formed in air at room temperature, the thickness of these oxides is in the range 2–5 nm; however, this thickness can be increased by anodic oxidation [2, 3], thus leaving the metallic material in the so-called passive state. A living organism, containing saline solutions, is considered to be a corrosive medium for several metals, so that the durability of implants critically depends on the metallic-material corrosion resistance, which in turn is determined by the physicochemical properties of the surface oxide.

Studies done in our laboratory [4–7] on the stability of oxides grown anodically on Ti–50Zr at.%, Zr–2.5Nb wt%, and Ti–13Nb–13Zr wt%, in aerated Ringer physiological solutions, indicate that the stability of these oxides is increased by keeping them under constant-potential conditions until a quasi-stationary current is reached, but decreased by the presence of chloride ions in the electrolyte during the anodizing process. We also reported that Ti–50Zr presents better corrosion protection than Zr–2.5Nb or pure Zr in some solutions simulating physiologic media [Ringer and PBS (phosphate buffered saline) solutions] [4]; additionally, when the stability of oxide films grown on Ti–50Zr in acid electrolytes (pH $\approx$1) was compared in a Ringer solution, the stablest films were clearly the ones obtained in H_2SO_4 [7]. Interestingly, no corrosion evidence could be found for anodized Ti–13Nb–13Zr in chloride solutions even at potentials as high as 8 V (vs. SCE), while Ti–50Zr underwent localized corrosion (pitting corrosion) at potentials lower than 2 V [6].

The surface microtexture and the chemical composition of an implant biomaterial play an important role in

L. T. Duarte · S. R. Biaggio (✉) · R. C. Rocha-Filho · N. Bocchi
Departamento de Química, Universidade Federal de São Carlos, C.P. 676, São Carlos, SP 13566-970, Brazil
e-mail: biaggio@ufscar.br

promoting its osteointegration [8, 9]. Thus, surface modification of titanium and its alloys using laser or electrochemical oxidation techniques has been the focus of many works, resulting in information on the biological response [10–12] and the characterization of the modified layer [9, 11]. Micro-arc electrochemical oxidation (MAO) of titanium, i.e., Ti oxidation under spark production at very high voltages, causes the formation of a very porous oxidized surface that favors direct contact between bone and implant [12].

In order to increase biocompatibility, biocompatible ceramics have been coated on oxidized Ti and Ti alloys, which can then be used in either orthopedic or dental implants. Among the bioactive materials are the bioglasses, the glass and the calcium-phosphate-type ceramics; this latter group has hydroxyapatite (HA) –$Ca_{10}(PO_4)_6(OH)_2$– as its most widely employed material [13–16].

Several methods have been employed in order to prepare HA coatings. Among them, electrochemical deposition is a good choice to quickly obtain uniform HA coatings on substrates of complex shapes at room temperature; furthermore, this method allows the control of the film thickness and composition [17]. Recently, we reported that the corrosion resistance of Ti–13Nb–13Zr is increased by HA electrodeposition on the fresh polished surface of this alloy [18]. Apatite coatings may also be obtained by the biomimetic method, in which HA precipitation conditions are adjusted to mimic the ones in the human body; hence the HA coating on different surfaces is expected to be more similar to the biological one [13]. Reiner and Gotman [19] coated titanium substrates with biomimetic calcium phosphate (Ca–P) and found different Ca–P phases as a function of substrate geometry and deposition time. On the other hand, Li et al. [14] reported a considerable improvement in the osteointegration capability of Ti implants by modifying their surface by MAO and concomitantly incorporating Ca and P ions into the anodic oxide layer.

Nevertheless, HA deposition on the promising Ti–13Nb–13Zr alloy has not been extensively explored, especially when an anodic oxide whose porosity may enhance osteointegration already protects the alloy. Besides that, there is very little information in the literature concerning the changes of electrochemical properties when a metallic biomaterial is coated with HA. Therefore, the aim of this work is to investigate the effect of electrochemically or biomimetically deposited HA coatings on the electrochemical properties of the Ti–13Nb–13Zr alloy prepassivated by a porous anodic oxide obtained by MAO. For such, the stability and the corrosion behavior of alloy/oxide and alloy/oxide/HA samples, kept in PBS solution, were monitored in situ during 49 days by electrochemical impedance spectroscopy (EIS) measurements. The morphology and structure of the HA coatings were analyzed before and after the immersion period by scanning electron microscopy (SEM) and X-ray diffraction (XRD).

2 Experimental

2.1 Alloy preparation

The samples of the polycrystalline Ti–13Nb–13Zr wt% alloy used in this work were produced at the Lorena School of Engineering of the University of São Paulo (EEL–USP), Brazil. Their preparation and characterization are partly described elsewhere [20, 21]. Alloy ingots, obtained by electric arc melting under an argon atmosphere in a water-cooled Cu crucible, were sequentially annealed at 1000°C for 1 h and water quenched. After, they were cold worked by swaging to obtain a 9 mm rod, which was again annealed at 1000°C for 1 h, followed by cooling in air. Working electrodes were made from disk-shape pieces of this Ti–13Nb–13Zr rod, exposing a geometrical area of about 1 cm^2 to the electrolyte. Previous to any use, the surface of the Ti–13Nb–13Zr electrodes was polished with sandpaper (silicon carbide grit 600) and rinsed with deionized (Milli-Q®) water. A conventional three-electrode cell was used in all electrochemical experiments; all solutions were always kept at room temperature (ca. 25°C). A saturated calomel electrode (SCE) was used as reference and a 2 cm^2 Pt foil was used as counter electrode.

2.2 Preparation of the coatings

First, anodic oxides were grown on the surface of the Ti–13Nb–13Zr electrodes by the MAO technique [22]: application of a cell voltage of 300 V for 60 s, in a phosphate solution (35.81 g l^{-1} Na_2HPO_4 + 13.80 g l^{-1} NaH_2PO_4) of pH 5. Hereinafter, these electrodes will be referred to as alloy/oxide samples.

Second, HA films were deposited on alloy/oxide samples by either an electrochemical or a biomimetic procedure. In the former, HA films were deposited by applying −13 mA cm^{-2} during 60 min, at 40°C, using an aqueous 137.8 mmol l^{-1} NaCl + 1.67 mmol l^{-1} K_2HPO_4 + 2.5 mmol l^{-1} $CaCl_2$ solution [18, 23]; hereinafter, these electrodes will be referred to as alloy/oxide/HA_{electr} samples.

In the biomimetic procedure, alloy/oxide samples were first immersed in an aqueous 5 mol l^{-1} NaOH solution, at 60°C, for 24 h, to increase the number of –OH terminations on the oxide surface [24]. Subsequently the HA film was deposited by immersion in simulated body fluid (SBF) solutions for 28 days, at 37°C. In the first day, this immersion was in a SBF solution: 8.053 g l^{-1} NaCl + 0.353 g l^{-1} $NaHCO_3$ + 0.224 g l^{-1} KCl + 0.174 g l^{-1} KH_2PO_4 + 0.072 g l^{-1} Na_2SO_4 + 0.278 g l^{-1} $CaCl_2$ + 0.305 g l^{-1} $MgCl_2{\cdot}6H_2O$ + 6.057 g l^{-1} $CNH_2(CH_2OH)_3$).

From the second day on, a 50% more concentrated SBF solution (1.5 SBF) was used; this solution was changed for a fresh one every 48 h. The pH of both SBF solutions was adjusted to 7.2 using HCl and tris(hydroxymetyl)aminomethane solutions [25]. Hereinafter, these electrodes will be referred to as alloy/oxide/HA_{biom} samples.

2.3 Electrochemical behavior

Several alloy/oxide, alloy/oxide/HA_{biom}, and alloy/oxide/HA_{electr} samples were immersed in an aerated PBS solution during 49 days at room temperature. From time to time, samples had their electrochemical properties analyzed by EIS measurements carried out in the same solution and keeping the samples at their open circuit potential. For these measurements, a 10 mV (rms) sinusoidal signal was applied in the 10 mHz to 10 kHz frequency range, using an Autolab PGSTAT30 potentiostat/galvanostat from Eco Chemie controlled by the FRA software.

2.4 Structural and morphological characterization of the coatings

The morphology and structure of the alloy/oxide, alloy/oxide/HA_{biom}, and alloy/oxide/HA_{electr} surfaces, before and after immersion in the aerated PBS solution, were analyzed by means of SEM micrographs and X-ray diffractograms obtained with a Philips XL30 FEG scanning electron microscope and a Rigaku Rotaflex RU-200B diffractometer, respectively.

3 Results and discussion

3.1 Structural and morphological characterization of the coatings

SEM and XRD were used to analyze many of samples; typical results are presented in Figs. 1 and 2.

From the micrograph for an alloy/oxide sample (Fig. 1a) it is clear that a very porous oxide film is formed using the MAO technique at 300 V, with pores (diameter in the 1–3 μm range) uniformly distributed on the oxide surface. On the alloy/oxide/HA_{biom} sample (Fig. 1b), the biomimetic apatite film presents a layered globular and very rough morphology; this film is uniform and thick enough to completely cover the underneath oxide. Similarly, on the alloy/oxide/HA_{electr} sample (Fig. 1c), the electrodeposited apatite film is also uniform, but presents smaller globules and roughness. The HA_{biom} globules are in the 10–20 μm range, while the HA_{electr} ones are in the 1–2 μm range. From these images, it is apparent that many HA_{biom} layers

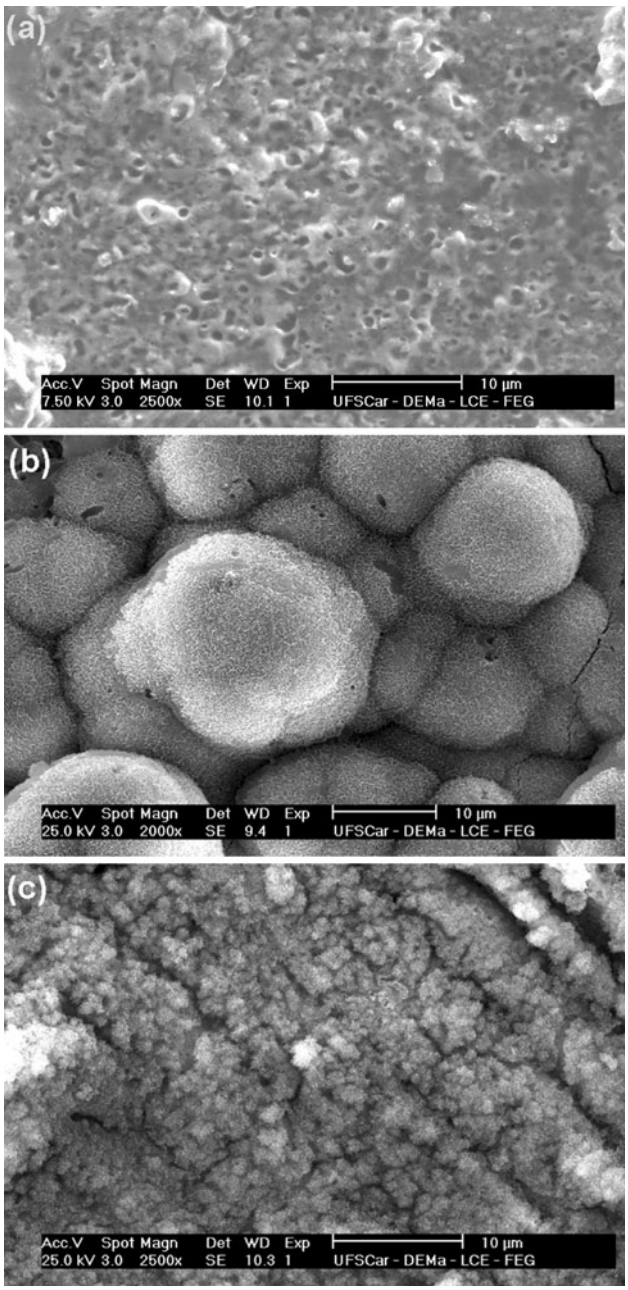

Fig. 1 SEM micrographs of the coatings on Ti–13Nb–13Zr: **a** alloy/oxide; **b** alloy/oxide/HA_{biom}; **c** alloy/oxide/HA_{electr}

(each about 10 μm thick) are deposited on the alloy. On the other hand, it could be inferred that only one layer of HA_{electr} is deposited, since it seems that the underneath oxide topography is preserved; this would imply a thinner film, at least 1 μm thick. Roughness and porosity presented by HA films on implant materials are positive features because they favor both osteointegration [15, 26] and drug delivery [26]. These features can also allow a strong interlacement between bone tissue and implant, increasing the in vivo mechanical resistance of the biomaterial [27].

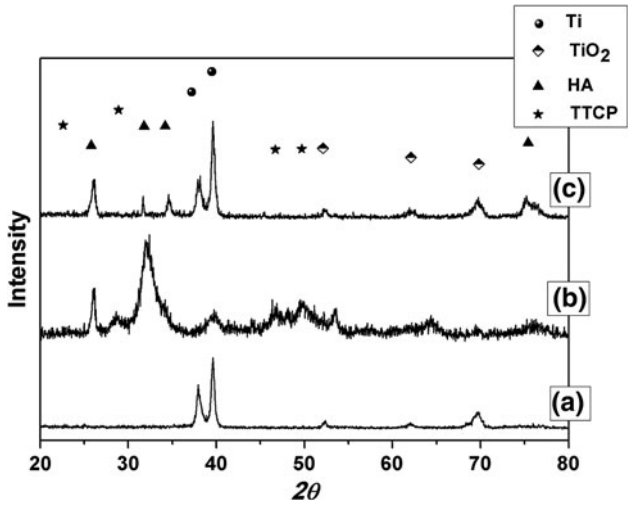

Fig. 2 X-ray diffractograms of the coatings on Ti–13Nb–13Zr: (**a**) alloy/oxide; (**b**) alloy/oxide/HA_{biom}; (**c**) alloy/oxide/HA_{electr}

Therefore, from the micrographs shown in Fig. 1 we conclude that both types of HA film deposited on the alloy/oxide surface present this roughness feature that is an important requirement for implant biomaterials.

X-ray diffractograms obtained for the different samples are shown in Fig. 2. Comparison of the 2θ data obtained for the alloy/oxide sample (Fig. 2a) with JCPDS standards (insert in the figure) allowed to conclude that the alloy is coated by TiO_2; the peaks at 38° and 40° are due to the major alloying element Ti in the substrate. For the alloy/oxide/HA_{biom} sample (Fig. 2b), the diffractogram presents wide bands around 26°, 29°, and 32°; these are characteristic of a large number of peaks due to many apatite phases and indicate a poorly-crystalline structure, similarly to biological apatite [25, 28]; the diffractogram also presents peaks related to tetracalcium phosphate—TTCP. Though more than one phase is commonly found in calcium phosphate coatings, this was not the case for the electrochemically deposited apatite. The diffractogram obtained for the alloy/oxide/HA_{electr} sample (Fig. 2c) reveals well-defined peaks at 26°, 32°, and 34°, which can be attributed to the crystalline HA phase, as previously observed for HA electrodeposited on a freshly polished Ti–13Nb–13Zr surface [18]. The corresponding Ti peaks are more intense than the ones in the diffractogram for the alloy/oxide/HA_{biom} sample (Fig. 2b), indicating that HA_{electr} is thinner than HA_{biom}. Therefore, though thicker coatings can be obtained by the biomimetic method, the electrodeposition technique yields more HA-like coatings. However, TTCP, present in HA_{biom}, has also been considered an interesting phase, because of its role in bone formation and the fact that it is a precursor of the HA phase [29].

3.2 Electrochemical behavior

EIS measurements were carried out for different samples as a function of their immersion time in the aerated PBS solution. As examples of typical results, EIS spectra obtained for the alloy/oxide and alloy/oxide/HA electrodes after 35 days of immersion are shown in Fig. 3. The electric equivalent circuit (EEC) method was employed to analyze all the acquired spectra, using a non-linear least squares program to find the best fit [30]. Figure 4 shows the EECs whose response best fitted the impedance data at any immersion time. Due to surface heterogeneities (high roughness for either the oxide or the HA films, as shown in Fig. 1), a constant-phase element Q was used to fit the data instead of a pure capacitor C; these circuit elements are directly related by $Q = Cw^{n-1}$, where w is the angular frequency and n a number varying between 0 and 1 ($n = 1$ for a pure-capacitor behavior) [31].

For the alloy/oxide/solution interface, the obtained response is typical of a bi-layer oxide (a porous outer layer

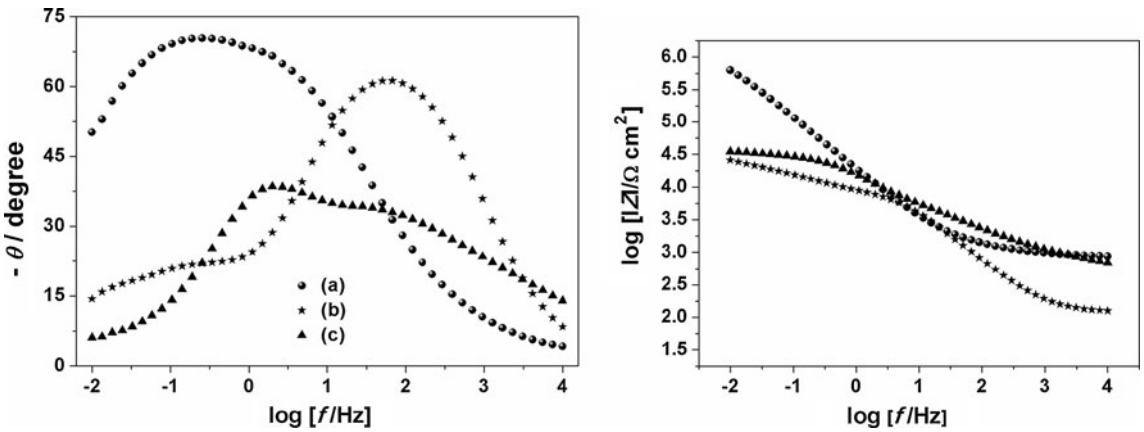

Fig. 3 Electrochemical impedance spectra (Bode diagrams) of the coatings on Ti–13Nb–13Zr after 35 days at open circuit in an aerated PBS solution: (**a**) alloy/oxide; (**b**) alloy/oxide/HA_{biom}; (**c**) alloy/oxide/HA_{electr}

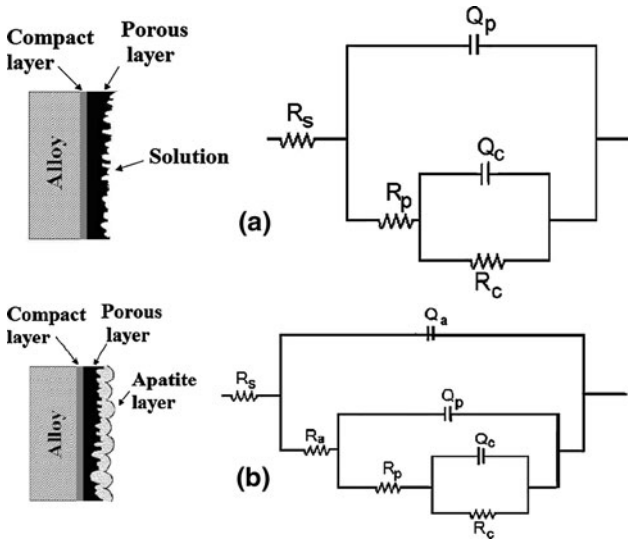

Fig. 4 Schematic representation of the **a** alloy/compact layer/porous layer/solution and **b** alloy/compact layer/porous layer/HA/solution interfaces, with the corresponding electric equivalent circuits whose responses were used to fit the respective EIS spectra

on an inner compact layer)—see EEC in Fig. 4a, represented as $R_s(Q_p[R_p(R_cQ_c)])$, where R_s is the resistance associated to the electrolyte solution relaxing at high frequencies, R_c and Q_c are the resistance and the constant-phase element associated to the compact oxide layer, and R_p and Q_p the resistance and the constant-phase element associated to the porous oxide layer. Badawy et al. [32], who investigated the electrochemical response of porous potentiostatically anodized titanium, also reported that the EIS spectra of the anodized Ti samples after immersion for up to 94 h in a phosphate buffer of pH 7.4 at 25°C could be fitted by the response of this EEC. Similarly, Souza et al. [33] reported that EIS data for potentiodynamically anodized Ti–13Nb–13Zr or Ti6Al4V in a Ringer solution were fitted by the response of this same EEC.

On the other hand, for the alloy/oxide/HA/solution interface (either HA_{biom} or HA_{electr}), the impedance response is typical of a tri-layer system—see EEC in Fig. 4b, represented as $R_s(Q_a[R_a(Q_p[R_p(R_cQ_c)])])$. Similarly to the previous circuit, the subscripts 'c' and 'p' for the R and Q elements denote compact and porous oxide layers, respectively, whereas the subscript 'a' refers to the apatite layer. It is clear from Fig. 3 that the apatite coatings modify considerably the impedance response of the system. By comparing the shifts in the phase-angle (θ) maxima, one can infer that the processes in the oxide are relaxing at the lower frequencies, while the processes in the apatite layer are relaxing at the highest frequencies. Badawy et al. [32] also reported EIS spectra that could be fitted by the response of this EEC, for anodized porous Ti samples that were immersed for 120 min (at 25°C) in a phosphate buffer of pH 7.4 containing different concentrations of Ca^{2+} ions; according to the authors, an additional layer was present on the anodized porous Ti due to adsorbed Ca^{2+} ions.

Table 1 presents the values obtained for the different elements of the EECs whose response fitted the EIS spectra for the alloy/oxide and alloy/oxide/HA electrodes, before and after their immersion in the aerated PBS solution. For both equivalent circuits, the chi-square (χ^2) distribution values were in the 10^{-3} to 10^{-4} range, which indicates good agreement between the simulated and experimental impedance responses. The lower Q_a values for the alloy/oxide/HA_{electr} sample (see Table 1) are consistent with a less rough surface, a feature already noted for HA_{electr} from the SEM micrographs. The slight decrease of the Q_a values for both HA films after immersion in the PBS solution indicates a slight surface flattening, probably due to film lixiviation. On the other hand, the R_c values varied significantly from the oxide layer only ($\geq$550 kΩ cm^2) to the oxide/HA layers (about 50 kΩ cm^2). This means that both apatite deposition methods interfere with the TiO_2 lattice of the inner (compact) layer in a way that changes its conductivity. For the

Table 1 Values for the different elements of the electric equivalent circuits (see text) whose response fitted the data obtained for the alloy/oxide, alloy/oxide/HA_{biom}, and alloy/oxide/HA_{electr} samples, before and after a 49-day immersion in the aerated PBS solution

EEC element	Alloy/oxide		Alloy/oxide/HA_{biom}		Alloy/oxide/HA_{electr}	
	Before	After	Before	After	Before	After
R_c/kΩ cm^2	580	550	50	45	46	59
Q_c/F cm^{-2} s^{n-1}	3.2×10^{-7}	2.6×10^{-7}	1.2×10^{-5}	1.8×10^{-5}	0.6×10^{-6}	1.2×10^{-6}
n_c	0.94	0.92	0.81	0.83	0.84	0.87
R_p/kΩ cm^2	38	34	27	16	35	19
Q_p/F cm^{-2} s^{n-1}	5.3×10^{-3}	6.3×10^{-3}	2.7×10^{-3}	3.2×10^{-3}	4.3×10^{-3}	3.1×10^{-3}
n_p	0.65	0.67	0.62	0.65	0.66	0.64
R_a/kΩ cm^2	–	–	10	40	17	14
Q_a/F cm^{-2} s^{n-1}	–	–	6.5×10^{-4}	4.5×10^{-4}	3.1×10^{-5}	2.0×10^{-5}
n_a	–	–	0.75	0.73	0.77	0.76

biomimetic deposition, the preliminary soaking in the NaOH solution might either affect the oxide structure or decrease its thickness. For the electrochemical deposition, the imposed cathodic current might introduce defects and rearrangements in the oxide lattice that decrease its resistivity. As expected, the resistance of the porous outer oxide layer R_p is much lower (about 35 kΩ cm^2) than that of the compact oxide layer; additionally, R_p does not show any important variation when this porous layer is coated with the apatites. Furthermore, Table 1 also shows that the Q_p values are many orders of magnitude higher than the Q_c values, which is consistent with the fact that the outer porous oxide layer provides a much larger area in contact with the electrolyte solution than the compact inner oxide. Besides that, the greater deviation from 1 for n_p again denotes the roughness of the outer porous oxide layer for all the analyzed systems, according to the relationship between Q and C mentioned above.

Finally, Fig. 5a shows a more detailed analysis of the dependence of the apatite layer resistance (R_a) with the immersion time in the aerated PBS solution. The R_a values for the alloy/oxide/HA$_{biom}$ sample are higher than the ones for the alloy/oxide/HA$_{electr}$ sample and increase with immersion time. This higher resistance is due to the greater thickness of the HA$_{biom}$ film, slowly and biomimetically grown on the oxide-covered alloy, compared to the smaller thickness of the HA$_{electr}$ film, electrochemically grown on an initially quite resistive oxide film (ca. 580 kΩ cm^2) that hinders the thickening of the HA film. The slow continuous increase of the resistance of the alloy/oxide/HA$_{biom}$ sample is probably due to structural changes in the HA film, or even its thickening in the PBS solution, which contains calcium and phosphate ions that favor apatite formation. Thus, considering the R_a data, we conclude that the biomimetic apatite film provides a better corrosion protection to the biomaterial.

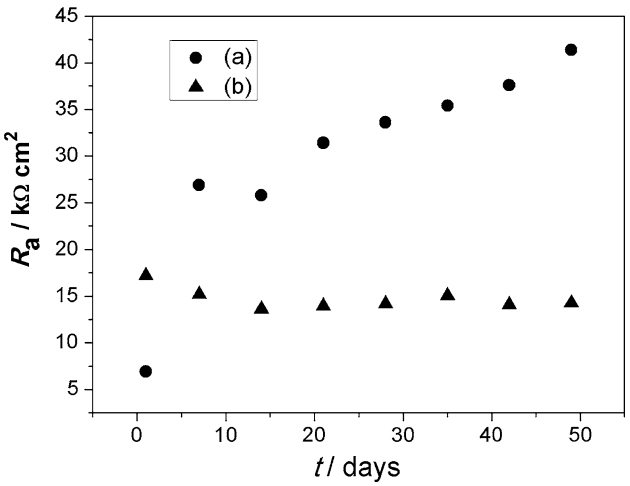

Fig. 5 Electric resistances of the apatite layers (R_a) of the coatings on Ti–13Nb–13Zr as a function of immersion time in an aerated PBS solution: (**a**) alloy/oxide/HA$_{biom}$; (**b**) alloy/oxide/HA$_{electr}$

3.3 Surface characterization after immersion in the PBS solution

SEM micrographs of the samples obtained after the 49-day immersion in the aerated PBS solution (Fig. 6) show different degrees of surface changes, depending on the coating. First, for the alloy/oxide sample, the less porous and flattened surface of the oxide (Fig. 6a; compare with Fig. 1a) indicates that a corrosion (or lixiviation) process occurred on the porous oxide layer, though much of it is still present on the alloy surface after 49 days in the PBS solution (the electric resistance of this sample decreased only about 5%). Second, for the alloy/oxide/HA$_{biom}$ sample (compare Fig. 6b with Fig. 1b), it is possible to conclude that no significant changes occurred on the HA$_{biom}$ coating after the long period in contact with the PBS solution. Finally, by comparing Fig. 6c with Fig. 1c and also with Fig. 6a, it becomes clear that the HA$_{electr}$ coating is the one that suffered the most important change, since just a few isolated areas of the apatite globules seem to remain on the oxide layer after the immersion in the PBS solution.

By comparing the diffractograms for alloy/oxide/HA$_{biom}$ before and after its immersion in the aerated PBS solution [diffractograms (b) in Figs. 2 and 7], one can conclude that the HA$_{biom}$ coating did not suffer any important structural changes as a consequence of its immersion in the PBS solution. The position of the diffraction peaks did not change; only a slight increase of the HA peak is present along with a consequent decrease of the TTCP peak. This indicates that some TTCP might have been converted to HA, which could explain the increase of the apatite layer resistance (R_a) observed as a consequence of the immersion in the PBS solution. On the other hand, from the comparison of the diffractograms for alloy/oxide/HA$_{electr}$ before and after its immersion in the PBS solution [diffractograms (c) in Figs. 2 and 7] one can infer that two of the four diffraction peaks for HA$_{electr}$ disappeared after the immersion in the PBS solution. This result, a consequence of lixiviation of the HA$_{electr}$ coating when exposed to the PBS solution, corroborates the previous SEM and EIS analyses.

From these results, we conclude that in the aerated PBS solution the HA$_{biom}$ coating is significantly stabler than the HA$_{electr}$ film, thus offering a better corrosion protection to the Ti–13Nb–13Zr alloy when in this solution.

4 Conclusions

Films of hydroxyapatite were successfully deposited by both the electrochemical (at constant cathodic current) and

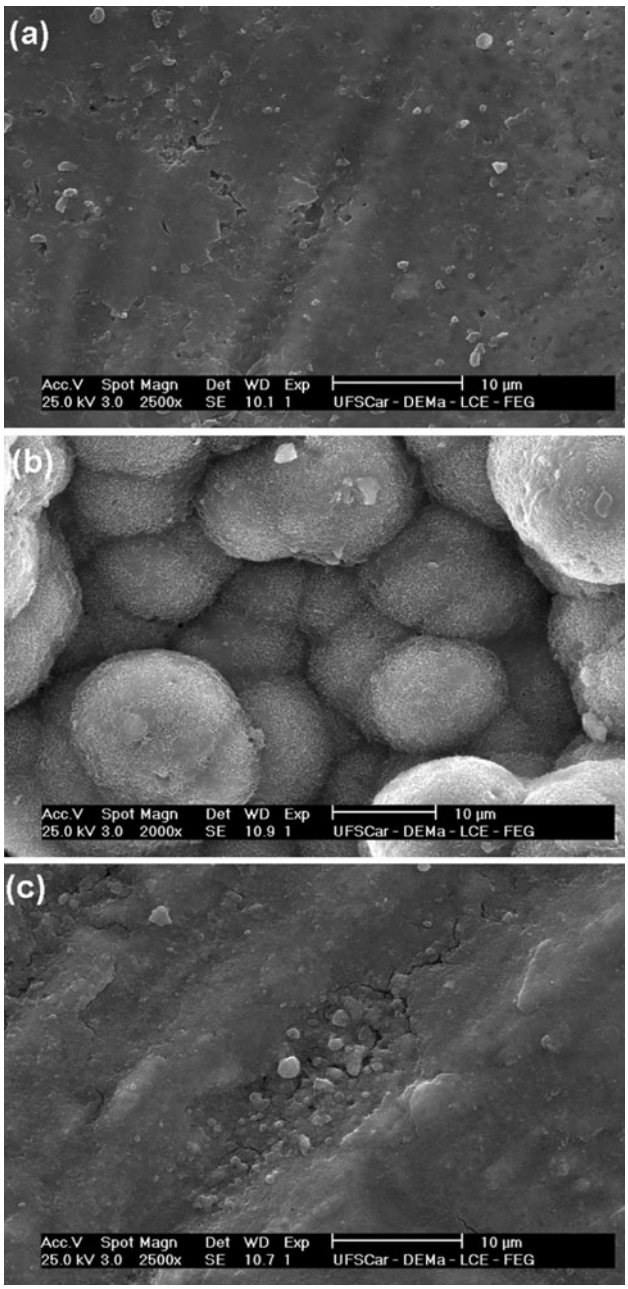

Fig. 6 SEM micrographs of the coatings on Ti–13Nb–13Zr after the 49-day immersion in an aerated PBS solution: **a** alloy/oxide; **b** alloy/oxide/HA_{biom}; **c** alloy/oxide/HA_{electr}

the biomimetic method on the Ti–13Nb–13Zr alloy pre-passivated by an anodic oxide film grown by micro-arch oxidation (MAO) at 300 V. This porous oxide provided a convenient substrate that promoted the deposition of highly adherent HA films, particularly attested by the HA_{biom} mechanical stability even after 49 days of immersion in the aerated PBS solution.

The application of both deposition methods yielded rough and globular apatite surfaces (globules in the

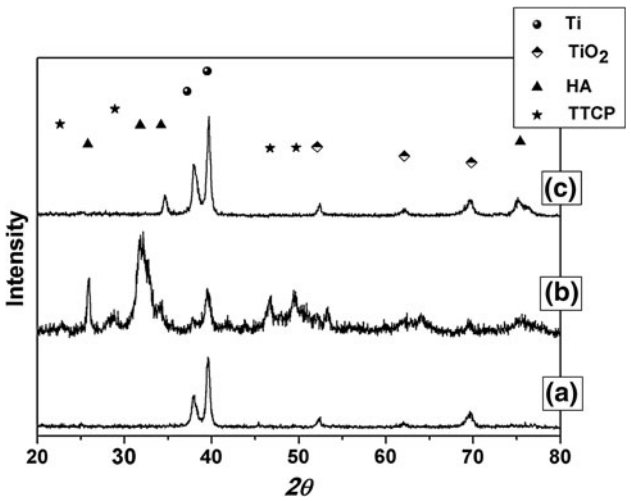

Fig. 7 X-ray diffractograms of the coatings on Ti–13Nb–13Zr after the 49-day immersion in an aerated PBS solution: (**a**) alloy/oxide; (**b**) alloy/oxide/HA_{biom}; (**c**) alloy/oxide/HA_{electr}

10–20 µm range for HA_{biom} and in the 1–2 µm range for HA_{electr}), which are important features when such a material is used in implants, since surface heterogeneities favor osteointegration.

From XRD data it was possible to infer that the electrochemical method yielded more biologic-like apatite films, while the biomimetic method yielded a film containing a mixture of calcium phosphate phases. Nevertheless, considering that after immersion for 49 days in the aerated PBS solution the biomimetically deposited film presented smaller variations in thickness and morphology, as well as a higher electric resistance, we conclude that the HA_{biom} film offers significantly greater protection to the Ti–13Nb–13Zr alloy when immersed in the PBS solution.

Acknowledgments Prof. Dr. Sandra G. Schneider (EEL–USP) is gratefully acknowledged for preparation of the alloy. Financial support and scholarships from the Brazilian funding agencies CNPq (National Council for Scientific and Technological Development) and CAPES (Coordination for Improvement of Higher Education Personnel) are also acknowledged.

References

1. Kobayashi E, Matsumoto S, Yoneyama T, Hamanaka H. Mechanical properties of the binary titanium-zirconium alloys and their potential for biomedical materials. J Biomed Mater Res. 1995;29:943–50.
2. Lohrengel MM. Formation of ionic space charge layers in oxide films on valve metals. Electrochim Acta. 1994;39:1265–71.
3. Marino CEB, Oliveira EM, Rocha-Filho RC, Biaggio SR. On the stability of thin-anodic-oxide films of titanium in acid phosphoric media. Corros Sci. 2001;43:1465–76.
4. Oliveira NTC, Biaggio SR, Rocha-Filho RC, Bocchi N. Electrochemical studies on zirconium and its biocompatible alloys Ti–50Zr at.% and Zr-2.5Nb wt% in simulated physiologic media. J Biomed Mater Res. 2005;74A:397–407.

5. Oliveira NTC, Biaggio SR, Piazza S, Sunseri C, Di Quarto F. Photo-electrochemical and impedance investigation of passive layers grown anodically on titanium alloys. Electrochim Acta. 2004;49:4563–76.
6. Oliveira NTC, Ferreira EA, Duarte LT, Biaggio SR, Rocha-Filho RC, Bocchi N. Corrosion resistance of anodic oxides on the Ti–50Zr and Ti–13Nb–13Zr alloys. Electrochim Acta. 2006;51: 2068–75.
7. Ferreira EA, Rocha-Filho RC, Biaggio SR, Bocchi N. Corrosion resistance of the Ti–50Zr at.% alloy after anodization in different acidic electrolytes. Corros Sci. 2010;52:4058–63.
8. Geetha M, Singh AK, Asokamani R, Gogia AK. Ti based biomaterials, the ultimate choice for orthopaedic implants—A review. Prog Mater Sci. 2009;54:397–425.
9. Kurella A, Dahotre NB. Surface modification for bioimplants: the role of laser surface engineering. J Biomater Appl. 2005;20:5–50.
10. Chen J, Ulerich JP, Abelev E, Fasasi A, Arnold CB, Soboyejo WO. An investigation of the initial attachment and orientation of osteoblast-like cells on laser grooved Ti–6Al–4V surfaces. Mater Sci Eng. 2009;29C:1442–52.
11. Khosroshahi ME, Mahmoodi M, Tavakoli J. Characterization of Ti6Al4V implant surface treated by Nd:YAG laser and emery paper for orthopaedic applications. Appl Surf Sci. 2007;253: 8772–81.
12. Li LH, Kong YM, Kim HW, Kim YW, Kim HE, Heo SJ, Koak JY. Improved biological performance of Ti implants due to surface modification by micro-arc oxidation. Biomaterials. 2004; 25:2867–75.
13. Abe Y, Kokubo T, Yamamuro T. Apatite coating on ceramics, metals and polymers utilizing a biological process. J Mater Sci. 1990;1:233–8.
14. Li Y, Lee IS, Cui FZ, Choi SH. The biocompatibility of nanostructured calcium phosphate coated on micro-arc oxidized titanium. Biomaterials. 2008;29:2025–32.
15. Brendel T, Engel A, Russel C. Hydroxyapatite coatings by a polymeric route. J Mater Sci. 1992;3:175–9.
16. Zhu L, Ye X, Tang G, Zhao N, Gong Y, Zhao Y, Zhao J, Zhang X. Biomimetic coating of compound titania and hydroxyapatite on titanium. J Biomed Mater Res. 2007;83A:1165–75.
17. Park JH, Lee YK, Kim KM, Kim KN. Bioactive calcium phosphate coating prepared on H_2O_2-treated titanium substrate by electrodeposition. Surf Coat Technol. 2005;195:252–7.
18. Duarte LT, Biaggio SR, Rocha-Filho RC, Bocchi N. Influence of hydroxyapatite on the corrosion resistance of the Ti–13Nb–13Zr alloy. J Mater Sci. 2009;20:1009–15.
19. Reiner T, Gotman I. Biomimetic calcium phosphate coating on Ti wires versus flat substrates: Structure and mechanism of formation. J Mater Sci. 2010;21:515–23.
20. Donato TAG, Almeida LH, Nogueira RA, Niemeyer TC, Grandini CR, Caram R, Schneider SG, Santos AR. Cytotoxicity study of some Ti alloys used as biomaterial. Mater Sci Eng. 2009;29C:1365–9.
21. Niemeyer TC, Grandini CR, Pinto LMC, Angelo ACD, Schneider SG. Corrosion behavior of Ti–13Nb–13Zr alloy used as a biomaterial. J Alloys Compd. 2009;476:172–5.
22. Yerokhin AL, Nie X, Leyland A, Matthews A, Dowey SJ. Plasma electrolysis for surface engineering. Surf Coat Technol. 1999; 122:73–93.
23. Ban S, Maruno S, Arimoto N, Hanada A, Hasegawa J. Effect of electrochemically deposited apatite coating on bonding of bone to the HA-G-Ti composite and titanium. J Biomed Mater Res. 1997;36:9–15.
24. Rakngarm A, Miyashita Y, Mutoh Y. Formation of hydroxyapatite layer on bioactive Ti and Ti–6Al–4V by simple chemical technique. J Mater Sci. 2008;19:1953–61.
25. Kokubo T. Formation of biologically active bone-like apatite on meats and polymers by a biomimetic process. Thermochim Acta. 1996;280–281:479–90.
26. Komlev VS, Barinov SM. Porous hydroxyapatite ceramics of bi-modal pore size distribution. J Mater Sci. 2002;13:295–9.
27. Le Geros RZ. Biodegradation and bioresorption of calcium phosphate ceramics. Clin Mater. 1993;14:65–88.
28. Lopez-Heredia MA, Weiss P, Layrolle P. An electrodeposition method of calcium phosphate coatings on titanium alloy. J Mater Sci. 2007;18:381–90.
29. Feng QI, Cui FZ, Wang H, Kim TN, Kim JO. Influence of solution conditions on deposition of calcium phosphate on titanium by NaOH-treatment. J Cryst Growth. 2000;210:735–40.
30. Boukamp BA. A package for impedance admittance data-analysis. Solid State Ionics. 1986;18:136–40.
31. Macdonald JR. Impedance spectroscopy. Emphasizing solid materials and systems. New York: John Wiley & Sons; 1987.
32. Badawy WA, Fathi AM, El-Sherief RM, Fadl-Allah SA. Electrochemical and biological behavior of porous titania (TiO_2) in simulated body fluids for implantation in human bodies. J Alloys Compd. 2009;475:911–6.
33. Souza MEP, Lima L, Lima CRP, Zavaglia CAC, Freire CMA. Effects of pH on the electrochemical behavior of titanium alloys for implant applications. J Mater Sci. 2009;20:549–52.